THE JOURNAL OF PHYSICAL CHEMISTRY C
A JOURNAL OF THE AMERICAN CHEMICAL SOCIETY

pubs.acs.org/JPCC

Article

Nanoconfinement Allows a Less Active Cascade Catalyst to Produce More C_{2+} Products in Electrochemical CO_2 Reduction

Samuel V. Somerville, Peter B. O'Mara, Tania M. Benedetti, Soshan Cheong, Wolfgang Schuhmann, Richard D. Tilley,* and J. Justin Gooding*

Cite This: *J. Phys. Chem. C* 2023, 127, 289−299

Read Online

ACCESS | Metrics & More | Article Recommendations | Supporting Information

ABSTRACT: Enzymes with multiple distinct active sites linked by substrate channels combined with control over the solution environment near the active sites enable the formation of complex products from simple reactants via the confinement of intermediates. We mimic this concept to facilitate the electrochemical carbon dioxide reduction reaction using nanoparticles with a core that produces intermediate CO at different rates and a porous copper shell. CO_2 reacts at the core to produce CO which then diffuses through the Cu to give higher order hydrocarbon molecules. By altering the rate of CO_2 delivery, the activity of the CO producing site, and the applied potential, we show that the nanoparticle with lower activity for CO formation produces greater amounts of hydrocarbon products. This is attributed to a combination of higher local pH and the lower amount of CO, resulting in more stable nanoparticles. However, when lower amounts of CO_2 were delivered to the core, the particles that are more active for CO formation produce more C_3 products. The importance of these results is twofold. They show that in cascade reactions, more active intermediate producing catalysts do not necessarily give greater amounts of high-value products. The effect an intermediate producing active site has on the local solution environment around the secondary active site plays an important role. As the less active catalyst for producing CO also possesses greater stability, we show that nanoconfinement can be used to get the best of both worlds with regard to having a stable catalyst with high activity.

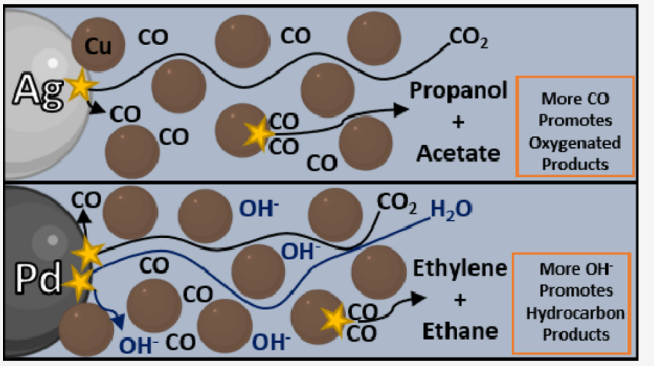

The electrochemical CO_2 reduction reaction (CO_2RR) has been studied extensively as an avenue for converting CO_2 into useful chemical fuels and feedstocks.[1,2] The CO_2RR can be split into two steps: (1) the initial reduction of CO_2 to CO and (2) the bimolecular reduction of CO to higher hydrocarbon products. Designing structures where CO formation and CO reduction occur at different active sites is appealing as Cu, the only known metal capable of catalyzing the formation of C_{2+} products, can do so from CO at significantly lower overpotentials than that from CO_2.[3,4] A few recent studies have therefore employed a "spill-over" mechanism where a highly active CO producing catalyst such as Ag is placed in proximity to a Cu surface.[5−10]

Our group has articulated the concept of a nanozyme as a nanoparticle that mimics the three-dimensional architecture of enzymes with active sites located inside substrate channels.[11] The definition of a nanozyme as not just a nanoparticle that performs the same reaction as an enzyme but instead incorporates some structural features of natural enzymes is beginning to be put forward.[12,13] This concept was applied to a cascade reaction with a Ag core-porous Cu shell nanoparticle where CO was produced on the Ag and subsequently confined within the porous Cu shell. Relating this AgCu system to naturally occurring cascade enzymes, the porous Cu shell was both the confining substrate as well as the second active site. This promoted the formation of propanol and other C_{2+} products at potentials as low as −0.65 V versus the reversible hydrogen electrode (RHE).[14] Nanoconfinement was key to the excellent performance of these AgCu nanozymes ensuring that intermediate CO was less likely to diffuse away from the electrode unreacted, resulting in high local CO concentrations in the Cu shell that facilitated the production of higher order hydrocarbons.[14] The high local CO concentrations, however, were shown to be responsible for the disintegration of the porous Cu shell at −0.8 V and more negative potentials. Hence, there is a decrease in C_{2+} product formation at these overpotentials.[15] The suggestion that the high local CO concentration was the reason for the Cu shell instability was

Received: October 26, 2022
Revised: December 18, 2022
Published: January 3, 2023

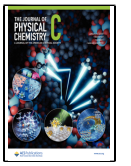

https://doi.org/10.1021/acs.jpcc.2c07518
J. Phys. Chem. C 2023, 127, 289−299

Scheme 1. Schematic Representation of the Proposed Concentrations of CO_2 (Purple) and How CO_2 Concentration Effects Reactions on the Core for the AgCu (a,c) and PdCu (b,d) at 5 (a,b) and 20 mL/min (c,d) CO_2 Flow Rates[a]

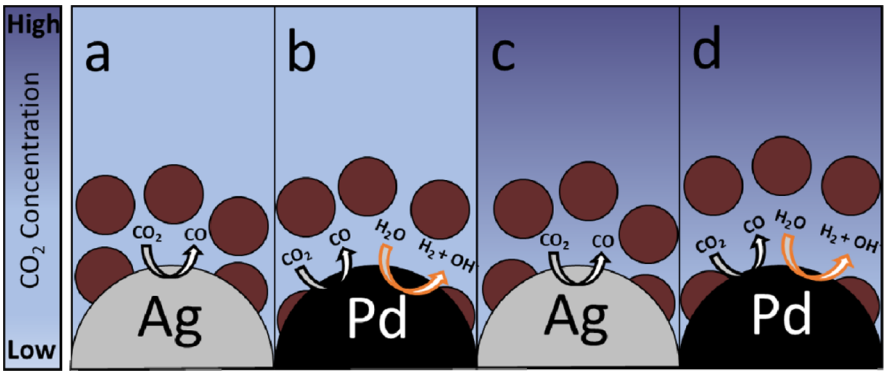

[a]Both the core metals' intrinsic CO activity and HER activity, as well as bulk CO_2 availability, influence the rate of each reaction and subsequent CO concentration and pH within the porous Cu shell. These solution conditions are directly related to the formed CO_2RR products.

supported by the replacement of the Ag core with a lower rate CO producing Pd core, resulting in a Cu shell that was stable at −0.8 V.[16,17]

The purpose of this paper is to explore how controlling the solution environment inside the nanoconfined spaces of the Cu shell can be used to control the product distribution. The solution environment is controlled by either using the flow rate of CO_2 altered by a mass flow controller purging the electrolyte through a gas dispersion tube to control the amount of reactant CO_2 delivered to the nanoparticles or by altering the metal of the core (Scheme 1). That is, changing the core from Ag to Pd alters the solution environment in two ways. The Pd core is less catalytically active for the reduction of CO_2 to the active intermediate CO due to stronger adsorption to CO and COOH compared with Ag but more active for the hydrogen evolution reaction (HER).[16−18] The former means that there is less CO intermediate than that with a Ag core for the reaction to higher order hydrocarbons in the Cu shell, and the latter means that with Pd, the pH in the porous shell will be higher than that with Ag due to the production of hydroxide during HER. The Pd core is overall more catalytically active when considering both the CO_2RR and HER but far less active than the Ag core for CO_2 reduction and formation of CO. This results in more charge being transferred overall on the Pd to produce OH^- increasing the local pH. Additionally, the higher gas generation of the Pd core could accelerate mass transport of reactants to the catalyst surface further influencing the pH in the confined shell.[19] However, due to the 35 nm thickness of the porous Cu shell, the local solution environment and pH cannot be directly measured. Taken together, by controlling the local pH value or CO concentration by altering the nanoparticle core material and the amount of CO_2 delivered to the nanoparticles, we were able to control product formation for a variety of important products and gain insights into how different conditions effect mechanistic pathways.

The illustration of the nanozymes in Scheme 1 showing a nanoparticle core with a porous copper shell illustrates the complexity of the system being investigated. In the experimental results shown in Figure 1, there are three main variables explored. These are first the overpotential, second, whether the core is Ag or Pd, and third, low versus high flow of CO_2 which surrogates for low versus high amounts of the reactant CO_2. The range of potentials explored was chosen

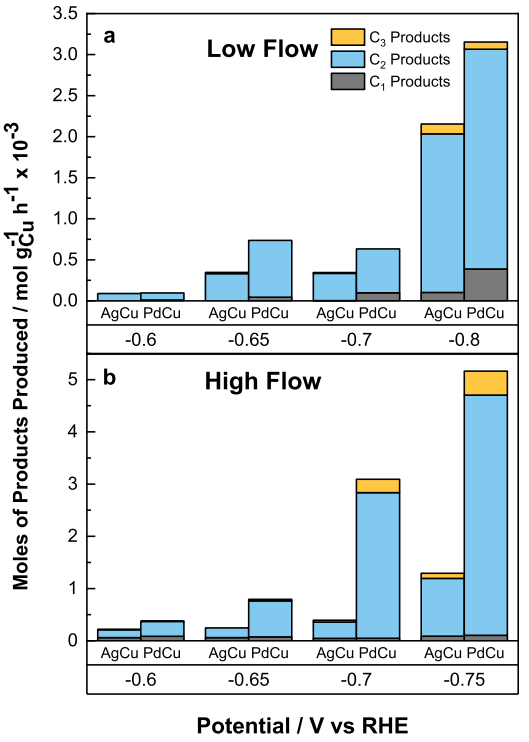

Figure 1. Moles of C_1, C_2, and C_3 products that form from the reduction of the CO generated at the core per gram of Cu at (a) −0.60, −0.65, −0.70, and −0.75 V vs RHE at 5 mL/min CO_2 flow rate, and (b) −0.6, −0.65, −0.7, and −0.8 at 20 mL/min CO_2 flow rate in a 1 h electrochemical experiment in 0.1 M $KHCO_3$ for the AgCu and PdCu nanozymes.

such that the reactant CO_2 must first diffuse through the nanoporous copper shell to the core where it reacts to produce CO. The CO then diffuses to the Cu active sites to generate higher-order hydrocarbons in a cascade reaction.

MATERIALS AND METHODS

Materials. The following chemicals were obtained from commercial suppliers and used without further purification. Poly(vinylpyrrolidone) Mn 55,000, sodium chloride (≥99.5%), sodium citrate tribasic dihydrate (≥99.0%), silver nitrate (≥99.5%), sodium borohydride (99%), palladium chloride (99%), L-ascorbic acid (≥99.0%), poly(ethylene

https://doi.org/10.1021/acs.jpcc.2c07518
J. Phys. Chem. C 2023, 127, 289−299

glycol) methyl ether Mn 5000, hydrazine solution 35 wt % in water, Nafion 117 solution (~5% in a mixture of lower aliphatic alcohols and water), methanol (HPLC grade), anhydrous dimethyl sulfoxide (≥99.9%), carbon monoxide, carbon dioxide, methane, ethane, ethylene, and acetylene were purchased from Sigma-Aldrich/Merck. Sodium hydroxide (≥98.0%), potassium hydroxide (≥99%), copper (II) nitrate (≥99.0%), ethanol (100%), and acetone (≥99.8%) were purchased from Chem-Supply Pty Ltd Australia. Nitric acid (69%) was purchased from VWR International Pty Ltd. Hydrochloric acid (32%) was purchased from ACI Labscan. Hydrogen peroxide solution (30%) was purchased from UNIVAR solutions. Deuterium oxide (99.9%) was purchased from Cambridge Isotope Laboratories Inc.

Potassium hydrogen carbonate (≥99.95%) was purchased from Sigma-Aldrich/Merck and purified using Chelex 100 sodium form 50−100 mesh (dry) that had been pre-treated with potassium hydroxide.

All glassware was rinsed with concentrated nitric acid and then Milli-Q water. All aqueous solutions were prepared using Milli-Q water.

Methods. *Ag Core Synthesis.* Ag cores were synthesized according to a literature procedure.[20] In a typical procedure, poly(vinyl pyrrolidone) Mn 55,000 (0.193 g) and $AgNO_3$ (0.193 g, 1.14 mmol) were dissolved in water (45.5 mL). To this solution, NaCl (454 μL, 5.0 M, 2.27 mmol) was added under magnetic stirring. Further stirring for 15 min in the dark led to the formation of a colloidal suspension of AgCl nanoparticles. Ascorbic acid (3.145 g, 17.9 mmol) and NaOH (0.929 g, 23.2 mmol) were dissolved in water (303.5 mL). To this solution, the freshly prepared AgCl colloid was added under magnetic stirring with further stirring for 2 h in the dark. During this step, the AgCl is converted to Ag. Using a centrifuge at 5000 rpm (4226 rcf) for 15 min, the reaction mixture was washed twice with water and concentrated to 50 mL. Poly(vinyl pyrrolidone) Mn 55,000 (0.100 g) was added to this stock solution, which was stored in the dark at 4 °C.

Pd Core Synthesis. Pd cores were synthesized according to a literature procedure.[21] In a typical procedure, a colloidal solution of Au seeds was prepared by dissolving $HAuCl_4{\cdot}3H_2O$ (10 mg, 29.4 μmol) in water (100 mL) with vigorous stirring, followed 1 min later by addition of aqueous trisodium citrate (1.0 mL, 1%). After an additional minute, $NaBH_4$ (1.0 mL, 0.075%) in aqueous trisodium citrate (1%) was added. The solution was stirred for 5 min and then stored at 4 °C until needed. A solution of H_2PdCl_4 (2.0 mM, 500 mL) was prepared by dissolving $PdCl_2$ (177.5 mg, 1 mmol) in HCl (500 mL, 4.0 mM) by stirring and heating (~80 °C) until solution turned clear orange-yellow. The solution was then allowed to cool, and the solid at the bottom filtered by gravity. H_2O_2 (20 mL, 30%) was added to the room-temperature stirring solution of H_2PdCl_4 (500 mL, 2.0 mM) and trisodium citrate solution (50 mL, 1% w/w). To this solution, 10 mL of the previously prepared Au seed solution was added. When the color changed from yellow to gray, corresponding to the Pd coating the Au seed, the solution was washed twice with PVP Mn 55,000 solution (20 g L^{-1}) and once with water. The solution was then concentrated to 50 mL and stored at 4 °C.

Porous Cu Coating on Ag Cores. Ag-core porous Cu-shell nanoparticles were synthesized using Ag cores synthesized, as previously described with a procedure modified from the literature.[22] In a typical procedure, Ag nanoparticles (30 mL of the previously prepared suspension) and $Cu(NO_3)_2$ (20 mL, 0.1 M) were added under stirring to an aqueous solution of poly(ethylene glycol) methyl ether Mn 5000 (2.4 g, 1.2 L, 2 wt %). To this solution, hydrazine (636 μL, 35 wt %) was added and left stirring for 3 min. Using a centrifuge at 4000 rpm (1878 rcf) for 15 min, the reaction mixture was separated, and the product was washed twice with water. Then, using a centrifuge at 5000 rpm (2935 rcf) for 15 min, the reaction mixture was washed twice with ethanol and dried at room temperature.

Porous Cu Coating on Pd Cores. Pd-core porous Cu-shell nanoparticles were synthesized using Pd cores synthesized, as previously described with a procedure modified from the literature.[22] Briefly, an aqueous solution of poly(ethylene glycol) methyl ether Mn 5000 solution (0.45 g, 225 mL, 2 wt %), the Pd nanoparticles (30 mL of the previously prepared suspension), and $Cu(NO_3)_2$ (3.75 mL, 0.1 M) were mixed under stirring. To this solution, hydrazine (119 μL, 35 wt %) was added and left stirring for 3 min. The reaction mixture was separated using a centrifuge at 4000 rpm (1878 rcf) for 15 min, and the product was washed twice with water. Thereafter, using a centrifuge at 5000 rpm (2935 rcf) for 15 min to collect the nanoparticles, the reaction mixture was further washed twice with ethanol and dried at room temperature.

Transmission Electron Microscopy. Transmission electron microscopy (TEM) samples were prepared by dropping 10 μL of concentrated colloidal dispersion of nanoparticles in ethanol onto carbon-coated Cu grids for low-resolution TEM and Au grids for high-resolution TEM (HRTEM) and allowing them to dry in air.

Low-resolution TEM analysis was performed on a FEI Tecnai G2 20 TEM.

HRTEM, scanning transmission electron microscopy (STEM), and energy-dispersive X-ray spectroscopy (EDX) analysis was performed on a JEOL JEM-F200 Multi-Purpose FEG-S/TEM.

Electrode Preparation. Plain carbon cloth-1071 HCB purchased from Fuel Cell Store, cut into pieces with a 1.5 × 1.5 cm^2 contact area were sonicated in acetone for 10 min, then methanol for an additional 10 min and dried at 40 °C. An ink suspension in methanol and 1% (v/v) Nafion 117 (5 wt % solution) was prepared with a concentration of 7.5 mg mL^{-1} of particles. A total of 240 μL of the ink was dropcast onto the carbon cloth in four 60 μL aliquots, with the carbon cloth clamped by self-closing tweezers. The cloth was turned over after each 60 μL aliquot to ensure uniform coverage, and the cloth was left to dry at room temperature, resulting in an overall loading of 1.8 mg of particles per cloth. This 1.8 mg of particles includes any surfactant still bound to the particle surface.

Electrochemical Setup. A custom low-volume H-cell was employed for all experiments, as shown in Figure S1. The low volume enhances the concentration of liquid products for further analysis by ^1H NMR. The cathode (with the working and reference electrode) and the anode (with the counter electrode) compartments of the H-cell were separated by a Fumasep anion exchange membrane, purchased from the Fuel Cell Store to stop products formed on the working electrode from being oxidized on the counter electrode. This membrane was stored in 0.1 M $KHCO_3$ when not in use.

The working electrode employed was the carbon cloth loaded with the nanozymes connected with a clip, and the reference electrode used was a custom-built Ag|AgCl|sat. KCl electrode. For every experiment, a new working electrode and

https://doi.org/10.1021/acs.jpcc.2c07518
J. Phys. Chem. C 2023, 127, 289−299

fresh electrolyte were employed. Carbon cloth (1071 HCB) purchased from the Fuel Cell Store was used as the counter electrode with dimensions of 3 × 5 cm. A constant potential was applied for 1 h using either an Autolab PGSTAT-12 potentiostat controlled with Nova 2.1.2 software, a BAS100W electrochemical workstation from BioAnalytical Systems Inc., or a CHI 660E electrochemical workstation. Inline gas product quantification was performed during the measurements, and liquid product analysis was performed before and after the measurements. CO_2 was supplied to the electrolyte by purging the solution with an Ace gas dispersion tube with a porous tip with porosity 70−100 μm.

Potentials were converted from Ag|AgCl|sat. KCl to RHE using the Nernst equation

$$E_{RHE} = E_{Ag|AgCl|sat.KCl} + 0.059 \times pH + E^0_{Ag|AgCl|sat.KCl}$$

where pH = 6.8 and $E^0_{Ag|AgCl|sat.KCl}$ = 0.199 versus the standard hydrogen electrode. Potentials were applied for 1 h with a measurement of the resultant current taken every second.

Before an experiment, a 540 μL aliquot of the electrolyte was taken as a blank from the 6540 μL volume initially placed in the cathode compartment. After electrochemistry, the remaining 6 mL of the electrolyte was collected. From this, another 540 μL aliquot was taken. Each sample was mixed with a 60 μL aliquot of a solution of DMSO in D_2O. The DMSO in D_2O solution was prepared by mixing D_2O (10 mL) with a known amount of DMSO (5 μL). The 600 μL NMR aliquots were investigated on a Bruker AVANCE III HD 400 MHz NMR with 64 scans and 16 s recycle delay, using DMSO as the internal standard. Product quantification was performed via the internal DMSO standard to determine the concentration of CO_2 reduction products.

The DMSO peak position was calibrated at 2.6 ppm and its integral calibrated to equal 1. All other product peaks were integrated in both the blank and the test sample. This includes ethanol, methanol, acetate, formate, acetone, and *n*-propanol. The blank integration was then subtracted from the test, and the intensity corrected for the number of hydrogens in the environments corresponding to each peak. The subsequent value was then multiplied by the amount of DMSO in the ^{1}H NMR sample before being extrapolated to the number of moles in the entire 6 mL of the electrolyte. An example NMR spectrum is presented in Figure S2.

Gas products formed during CO_2 reduction were analyzed by inline gas chromatography (GC) using a SRI 8610C multiple gas analyzer #5 gas chromatograph column purchased from SRI Instruments calibrated using carbon monoxide, carbon dioxide, methane, ethane, ethylene, and acetylene [1% (w/w) each component in nitrogen aerosol of 4 L, analytical standard]. Hydrogen calibration was performed using a gas mixture of carbon monoxide, carbon dioxide, hydrogen, methane, and oxygen [1% (w/w) each component in nitrogen, cylinder of 14 L, analytical standard]. Four automatic 1.0 mL of gas injections (one every 14 min) were taken over the course of the 1 h electrochemical experiment. Of these four injections, the second was taken as representative and extrapolated to the hour-long run to find the total number of moles of gas products produced. This was conducted by calculating the moles in the injection based on the calibration, then multiplying by either 5 or 20 to account for the 5 or 20 mL/min flow rate and then 60 to account for the hour-long experiment. An example GC chromatograph is given in Figure S3.

Inductively Coupled Plasma−Optical Emission Spectroscopy. Inductively coupled plasma−optical emission spectroscopy (ICP−OES) was performed on both the AgCu nanozymes and PdCu nanozymes from a 100 μL aliquot of the methanol-Nafion ink used for preparing the electrodes. The dry AgCu nanozymes were digested in 1 mL of concentrated nitric acid (69%). The dry PdCu nanozymes were digested in 1 mL of aqua-regia. Both samples were heated at 80 °C for 1 h and then diluted in 9 mL of Milli-Q Water (one part aqua-regia solution to nine parts water). The samples were analyzed using an Optima7300DV ICP−OES PerkinElmer instrument.

RESULTS AND DISCUSSION

The nanozymes were prepared following a method described previously.[20−22] Briefly, Ag cores with 65.3 ± 8.8 nm and the Pd cores with 68.1 ± 14.2 nm diameter[20,21] were synthesized and then coated with a porous polycrystalline Cu shell using methods adapted from the literature (see the Methods section).[22] Note the large core sizes and shell were chosen deliberately to avoid additional effects on the catalytic activity such as lattice strain and alloying that influences the adsorption of reactants. Such effects are only observed with much smaller nanoparticles and thinner shells.[23−25] From TEM analysis, the Cu shell had a thickness of 34.2 ± 6.4 nm on the Ag core and of 35.1 ± 7.3 nm on the Pd core. The Cu crystallite diameter was similar for both the AgCu and PdCu nanozymes at 21 ± 4 and 23 ± 4 nm, respectively (Figure S4). The equivalent shell thickness and Cu crystallite size ensure similar diffusional environments for the reactant CO_2 to enter and for the confined intermediate CO and hydrocarbon products to leave the Cu shell. The same mass of nanozymes was then drop cast onto carbon cloth electrodes for the electrochemical CO_2 reduction measurements in a 0.1 mol L^{-1} $KHCO_3$ electrolyte. Chronoamperograms were recorded for the duration of 60 min at potentials between −0.6 and −0.8 V versus RHE (Figures S5−S8).

The dependence of the applied potential on the products generated from the reduction of CO on the Cu shell for both AgCu and PdCu nanozymes at the lower CO_2 flow of 5 mL min^{-1} is shown in Figure 1a. A detailed breakdown of each product with uncertainties can be found in Figure S9. The moles of products produced on each nanozyme were normalized by the mass of Cu (the secondary active site in the cascade) to elucidate the extent to which each core effect on the solution environment affects product formation. A detailed breakdown of the content of each metal on the electrode is shown in Table S1. The moles of product generated was chosen to retain kinetic information which is lost when normalized by Faradaic efficiency.

The results suggest that the local CO concentration and solution environment inside the nanoconfined porous space have a large effect on product formation. We suggest this as the Ag cores produce more CO than the Pd cores. For both Ag and Pd core nanozymes, similar amounts of C_2 products are obtained at the lowest and highest overpotentials (−0.6 and −0.8 V, respectively). At the lower overpotential, this is likely due to the relatively low production rate of CO on both Ag and Pd cores, and at higher overpotential, CO_2 begins to be more easily reduced directly on the porous Cu shell. This limits the mass transport of CO_2 to the core at higher overpotentials. The observations are quite different at

https://doi.org/10.1021/acs.jpcc.2c07518
J. Phys. Chem. C 2023, 127, 289−299

Scheme 2. Simplified Mechanisms for the Reduction of CO on a Cu Surface[a]

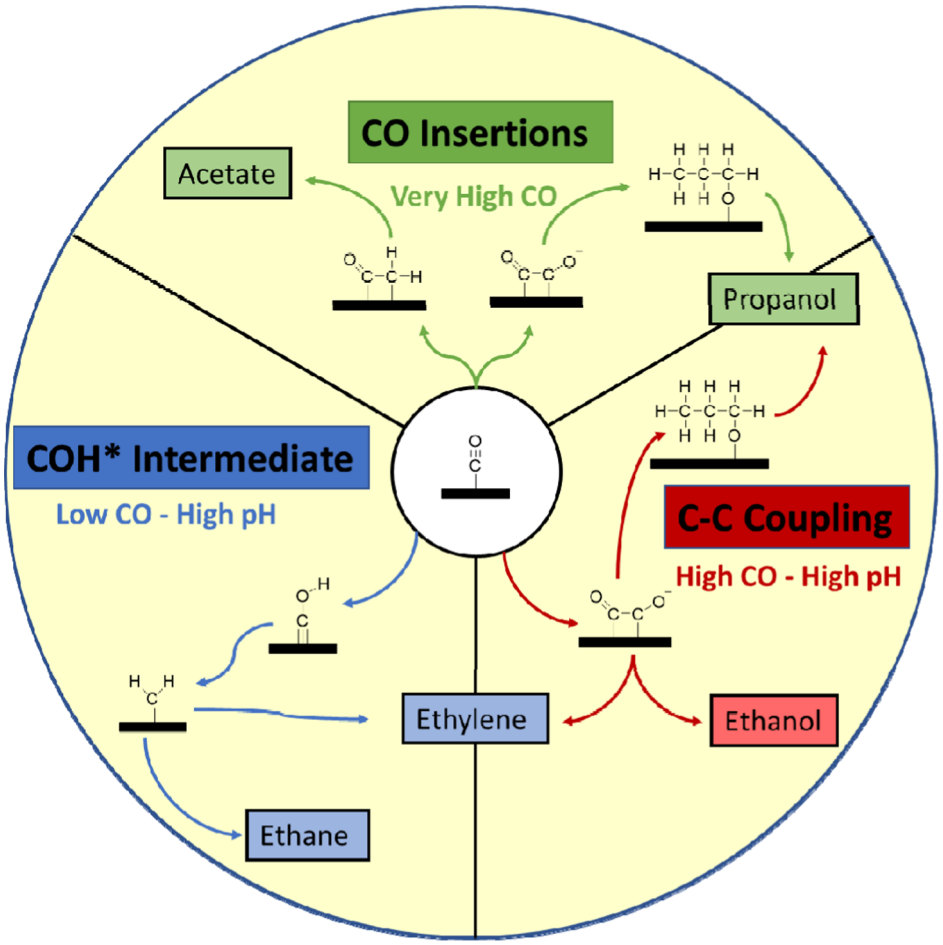

[a]The top (green) pathway corresponds to products forming at the highest CO concentration promoting the formation of products that form through a CO insertion mechanism. The left pathway (blue) corresponds to products with enhanced formation under high pH and low CO concentrations which are hydrocarbon products. The right pathway (red) corresponds to products that form with high pH and high CO concentration.[29,33,34]

intermediate potentials for both the AgCu and PdCu nanozymes. At −0.65 V, a significantly larger amounts of C_{2+} products were obtained with the PdCu nanozyme than that with the AgCu nanozyme even though the rate of CO_2 conversion of CO was higher with the Ag core.[2] As we will discuss in more detail below, a possible explanation for the greater amount of C_{2+} products with the Pd core may be related to the increased local pH with these particles in the nanoconfined Cu shell due to the higher rate of the HER at Pd relative to Ag.[26,27]

Interestingly, while C_2 products were the predominant species generated with both nanozymes, only the AgCu nanozymes gave a small amount of C_3 products at both −0.65 and −0.7 V at low flow, see the Supporting Information for zoom-in of the low overpotential region and more detailed product distribution with uncertainties (Figures S9 and S10). This small amount of C_3 product formation is significant if compared to the PdCu nanozyme which does not produce C_3 until a 150 mV higher overpotential is reached. It has been suggested that to produce C_3 products at such low overpotentials requires high CO concentrations and surface coverage.[28,29]

For both the AgCu and PdCu nanozymes, the total amount of C_{2+} produced remained similar at −0.7 V when compared to −0.65 V. We know from previous work that the PdCu nanozyme is stable in these conditions,[15] so the decrease in the amounts of products for the PdCu nanozyme at −0.7 V is not due to nanozyme degradation. It is therefore prudent to ask if the stagnation in the amount of product formation at −0.7 V for the PdCu nanozymes is due to the delivery of CO_2 to the core not being sufficient for the cascade to proceed optimally or the depletion of CO_2 in the electrolyte?

To answer this question, the flow of CO_2 to the electrolyte was increased from 5 to 20 mL/min. Figure 1b shows that increasing the CO_2 flow to 20 mL min^{-1} has a significant effect on the overall amount of C_{2+} products formed for both the AgCu and PdCu nanozymes. A detailed breakdown of each product with uncertainties can be found in Figure S10. Based on the observation that the CO_2 flow affects the product formation, we suggest that during CO_2 reduction conditions, the rate of CO_2 consumption at 5 mL/min is high enough to deplete CO_2 faster than it can be replenished. At the higher CO_2 flow, there are a number of important observations relative to the lower rate of flow. First, the PdCu nanozymes are now producing a significantly higher amounts of products than the AgCu nanozymes. Second, the PdCu nanozymes generate much more products at higher CO_2 flow than that at the lower CO_2 flow at every potential measured. This includes

https://doi.org/10.1021/acs.jpcc.2c07518
J. Phys. Chem. C 2023, 127, 289−299

an increase in C_{2+} product formation with increasing overpotential. This indicates that delivery of CO_2 was a limiting factor at the lower CO_2 flow. Third, unlike at low CO_2 flow, the PdCu nanozymes were also able to generate C_3 products. In contrast, for the AgCu nanozyme, the product generation was relatively similar at both high and low flow, with little change until −0.75 V.

Overall, the PdCu nanozyme outperforms the AgCu nanozyme at −0.65 V and more negative potentials for overall product formation at a higher CO_2 flow even though Pd is less active for CO formation than Ag. This higher C_2 product formation is not due to significantly higher current densities as the current densities are similar (Figures S5−S8) or more catalyst on the electrode (Table S1). At the lower CO_2 flow, and therefore lower CO_2 concentration, we observe a trade-off within a potential window around −0.65 V for both nanozymes of more overall hydrocarbon products for the lower CO production (PdCu) versus production of C_3 products for the higher CO production (AgCu). This trade-off is no longer observed at higher CO_2 flow with both C_2 and C_3 product formation increasing for the PdCu nanozymes with increasing overpotential.

Before discussing the results, we first highlight the impact of the three variables on the solution conditions that occur in the nanoconfined spaces within the porous copper shell. We do this as the reader will be well versed in understanding the impact of applied potential and the core catalytic activity on product generation but maybe less conversant with the impact of these variables on the solution conditions which are amplified with nanoconfinement. It is the changes in the solution inside the nanoconfined spaces that we feel are playing a large role in determining the product distribution from the CO_2RR in this system. We have shown previously with PtNi nanoparticles with nanoconfined channels exhibiting restricted diffusion into and out of nanoporous spaces can result in a very different solution environment to the bulk solution, affecting the electrocatalytic activity.[30]

The nanoconfinement in the nanoporous copper shell serves to concentrate the intermediates and products near the Cu active sites, while the reactions that proceed at the cores and shells also change other solution variables. For example, by changing the core material from more catalytically active Ag to the less active Pd, the amount of CO produced, and that will reside in the nanoconfined solution environment, will decrease. However, Pd is much more catalytically active for the HER. The faradaic efficiency for H_2 for both nanozymes can be found in Figure S11. This results in a more dramatic increase in pH within the nanoconfined porous Cu for the PdCu nanozyme than the AgCu nanozyme. This increase in the local OH^- concentration could also increase the rate of the non-Faradaic reaction of CO_2 and OH^- further decreasing the formation of CO on the core. However, it has been demonstrated that nanoconfined geometries limit diffusion of HCO_3^- limiting the neutralization of OH^- further increasing the local pH.[31,32] The different cores were therefore chosen as a way of modulating both the solution pH and the amount of CO intermediate produced, and consequently, the concentration of intermediate near the copper active sites where bimolecular reactions produce higher order hydrocarbons. Due to the intrinsic properties of the metal cores, high pH and low CO concentrations occur on the PdCu, while lower pH and high CO concentrations occur on the AgCu. The different rate of CO_2 flow determines the amount of CO_2 that reached the cores and therefore how much CO could be produced at a given potential. The different potentials then influenced the driving force for reactions to produce both the CO intermediate at the core and the higher-order hydrocarbon products at the copper shell. Together these variables allow us to define three main sets of solution conditions in the nanoconfined solution environment that influence the product distribution generated at the copper surface. We refer to these as (1) high CO and high pH which favors C_2 product formation alongside C_3 products, (2) low CO and high pH which favors hydrocarbon products such as ethylene and ethane, and (3) very high CO which favors insertion reactions, as illustrated in Scheme 2. We will discuss how we arrive at these suggested reactions in each regime below.

First, looking at the lower flow of 5 mL/min of CO_2 at the different product distributions observed with the AgCu and PdCu nanozymes, the three main observations are that the PdCu nanozymes produce more hydrocarbons and produce more C_1 products, and the AgCu nanozymes produce more C_3 products. The greater amount of hydrocarbon products with the Pd cores was at first a surprise to us because the Pd core is less active in producing the CO intermediate than the Ag. However, we propose that the elevated pH caused by the Pd core is responsible for the greater production of C_2 hydrocarbons. Chan and co-workers[35] have shown that an increase in pH from 7 to 13 lowers the energy of the rate-limiting proton transfer for C_2 products (OCCO*−OCCOH*). This causes a +300 mV shift in the C_2 product formation, resulting in an increase in C_2 product formation at the lower overpotentials used herein. Furthermore, others have ascribed an increase in C_2 selectivity at high alkalinity to the fact that going from a bound CO* to the C_1 intermediate CHO* is pH dependent and occurs less at high pH. Therefore, the pH-independent step of CO dimerization becomes more favored and results in more C_2 products.[3,27,36] These observations explain the higher C_2 product formation at the PdCu nanozymes relative to the AgCu nanozymes but do not explain the higher amount of C_1 with the PdCu. To understand the increase in C_1 product formation with the PdCu nanozyme, we can look to the products formed in the direct reduction of CO_2 on Pd metal. At −0.81 V, Pd metal has a faradaic efficiency of 2.9 and 2.8% for methane and formate, respectively.[2] From this, the higher C_1 product formation can be attributed to direct CO_2 reduction to methane at the Pd.

The other difference between the Ag and Pd cores to explain is the higher preponderance of C_3 products with the AgCu nanozymes at low CO_2 flow. The formation of C_3 products involves a bimolecular reaction between C_2 and C_1 species which we, and others, have proposed previously is facilitated by high local CO concentrations (the insertion regime in Scheme 2) which is the case for the AgCu nanozymes with the much higher catalytic activity of Ag for conversion of CO_2 to CO compared with Pd.[15,29,37]

At the lower CO_2 flow, it is important to highlight that the differences in product distribution can all be attributed to the different cores and how the reactions at the cores alter the solution environment in the nanoconfined spaces adjacent to the Cu surface where the second step in the cascade reaction proceeds. Reinforcing this statement is the fact that at −0.8 V, both the AgCu and the PdCu nanozymes give similar product distributions which are consistent with the reactions just occurring at the copper shell, and therefore, the composition of the core has minimal bearing on the products.

https://doi.org/10.1021/acs.jpcc.2c07518
J. Phys. Chem. C 2023, 127, 289−299

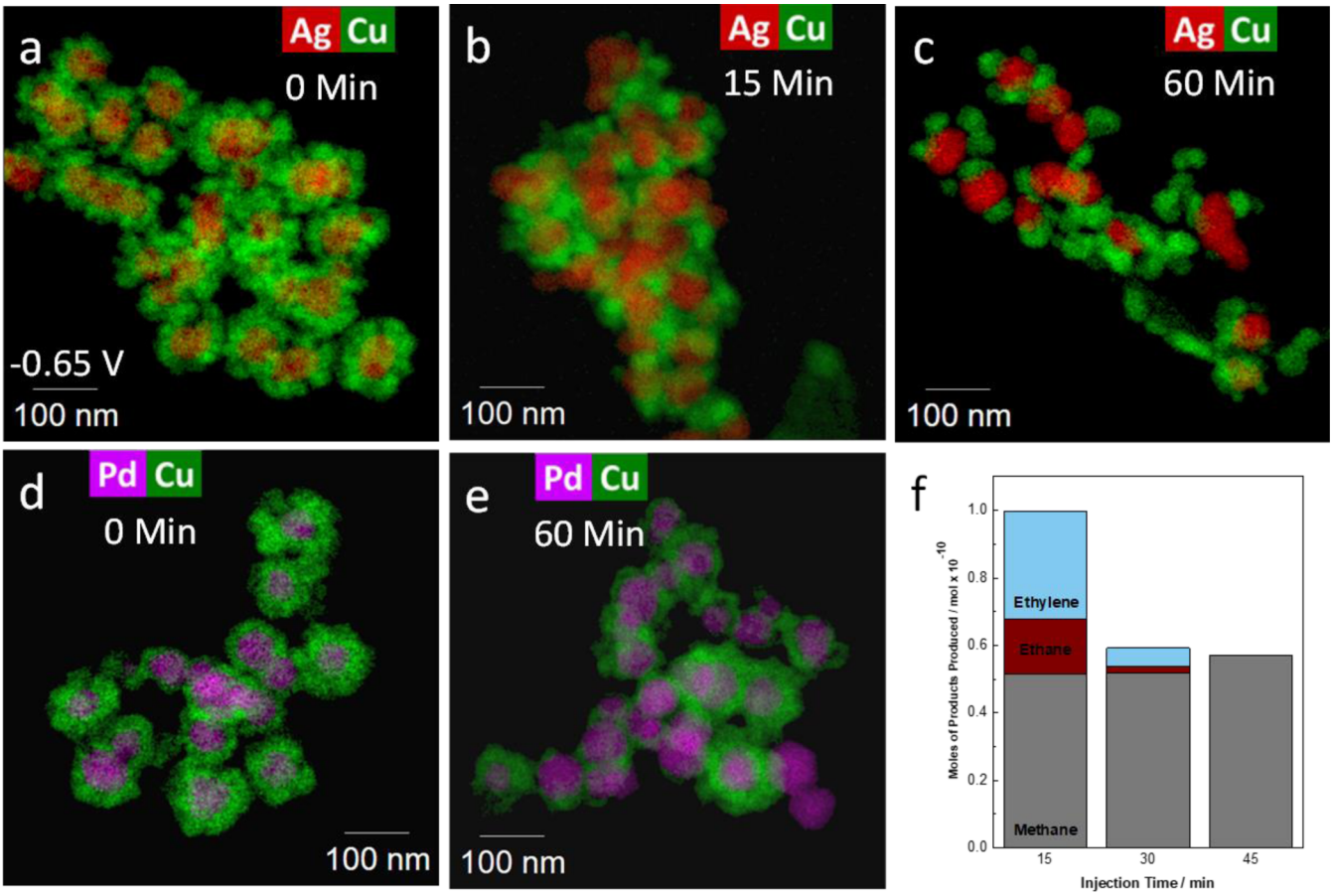

Figure 2. EDX maps of the AgCu and PdCu nanozymes over time, (a) pristine AgCu, (b) AgCu after 15 min, (c) AgCu after 60 min, (d) pristine PdCu, (e) PdCu after 60 min of catalysis at −0.65 V vs RHE with 20 mL/min CO_2 flow with Cu shown in green, Ag shown in red, and Pd shown in purple, and (f) moles of methane (gray), ethane (red), and ethylene (blue) in a single 1 mL of GC injection for the AgCu nanozyme during catalysis at 15, 30, and 45 min at −0.65 V vs RHE, note that the products correspond to the amount of products produced over a 3 s interval at corresponding time and not the accumulation of products up until that time.

We next turn our attention to the higher CO_2 flow of 20 mL/min, as shown in Figure 1b. Here again, there are three important observations. First, the PdCu nanozymes now generate a considerably higher amounts of products all round than the AgCu nanozymes. Second, the AgCu nanozymes generate very similar amounts of products at 20 mL/min CO_2 as they did at 5 mL/min CO_2. Finally, at the higher CO_2 flow, the PdCu nanoparticles now generate C_3 compounds at potentials more positive than −0.8 V.

Turning to the first two points, with higher delivery of the reactant to the electrode, one would expect more product generated as we see for the PdCu nanoparticles, and therefore, it is the absence of an increase in AgCu that caught our attention. Previous studies[15] have shown that the AgCu nanozyme structure is unstable at −0.8 V at the CO_2 flow of 5 mL min^{-1}. This instability was not due to applied potential but instead attributed to a high local concentration of CO causing the disintegration of the Cu shell.[15] This was demonstrated though the use of operando liquid cell TEM in combination with ex situ TEM. That study also determined that the PdCu nanozyme was more stable than the AgCu nanozyme at higher overpotentials. It is suggested that the unexpectedly low product formation observed for the AgCu nanozyme at higher CO_2 flow is due to the increasing bulk CO_2 concentration shifting the onset of the instability to less negative potentials.

In order to elucidate how the CO_2 flow and hence concentration and the rate of CO production affect nanozymes stability, TEM analysis of the particles after 1 h at −0.65 V and at a CO_2 flow of 20 mL min^{-1} was performed. These results are shown in Figure 2 with more images showing different regions of the sample found in the Supporting Information (Figures S12−S14).

The AgCu nanozymes at high CO_2 flow exhibited significant morphological changes throughout the electrochemical measurement with complete loss of the core−shell structure after 60 min at −0.65 V. Figure 2a shows the pristine AgCu nanozymes core−shell structures which began to fall apart after 15 min at −0.65 V (Figure 2b). After 15 min, the particle morphology became inconsistent with some AgCu particles losing the core−shell structure found in the pristine sample. However, in the 15 min sample, the Cu particulates were still localized around the Ag cores. After 60 min (Figure 2c), the core−shell structure had been destroyed for most particles. In comparison after 60 min at −0.65 V, the majority of the PdCu nanozymes, as shown in Figure 2e, still retained their porous Cu shell from the pristine sample (Figure 2d). As Cu instability in nanoconfined systems has been shown to be linked to higher CO concentrations, the PdCu nanozyme appearing more stable in the post-catalysis TEM demonstrates that the Pd core is not causing higher concentrations of CO than the Ag core,

https://doi.org/10.1021/acs.jpcc.2c07518
J. Phys. Chem. C 2023, 127, 289−299

reinforcing that other solution environment effects such as increased pH are likely the cause.[15]

The more dramatic structural changes observed with the AgCu nanozyme at high flow suggest that this instability is the cause of the lower amounts of complex products formed with these particles relative to the PdCu particles that retain their structure. To verify this, we attempted to correlate how the hydrocarbon molecules produced by the particles changed as a function of time. To do this, we looked at the gaseous products as, unlike the liquid products, they do not accumulate in the reaction solution. That is the gaseous products allow us to get an understanding of the product formation at a specific moment in the measurement. Figure 2f shows the moles produced of methane, ethane, and ethylene at 15, 30, and 45 min for the AgCu nanozyme at 20 mL/min CO_2 flow. At 15 min, corresponding to Figure 2b, we see some formation of C_2 products which is attributed to reactions occurring at the Cu shell. This is consistent with TEM analysis that showed intact Cu shells at this point in the measurement. However, at 30 min into the electrochemical measurement, a sharp drop in C_2 product formation is observed corresponding to the destruction of the Cu shell. After 45 min, we see a complete absence of the production of C_2 species which as polycrystalline Cu on its own does not produce C_2 products at −0.65 V corresponds to the loss of the core−shell structure, as shown in Figure 2c.[38] This destruction of the Cu shell with the Ag core is in contrast to the PdCu core−shell particle where after 60 min at −0.65 V, the Cu shell is still intact such that the "spillover" mechanism can occur in the nanoconfined shell.

We next turn our attention to why we see C_3 products at the higher CO_2 flow with the PdCu nanozymes. With the previously stated viewpoint that to get C_3 products a higher amount of CO needs to be produced in proximity to C_2 intermediates (see the green CO insertion pathway in Scheme 2).[14,39] Therefore, it seems logical that with higher CO_2 flow, the PdCu nanozymes can start producing C_3 products. To gain evidence to support this assumption, we analyzed the amount of unreacted CO leaving the nanozymes, as shown in Figure 3. Note that these data come from a GC injection collected 15 min after the commencement of the electrochemical measurement. This time point was chosen as within 15 min the AgCu nanozymes predominantly retained their structure at −0.65 V and 20 mL/min, as shown in the TEM data in Figures 2b and S12, and therefore, the cascade is still occurring. It is therefore a relevant time frame to determine the nature of the cascade reaction occurring.

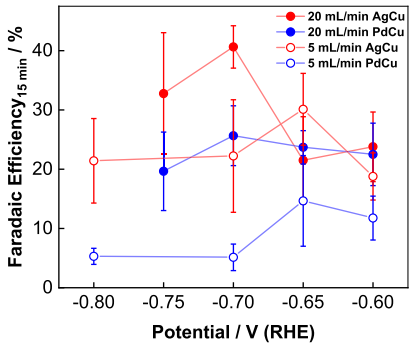

Figure 3. Faradaic efficiency for CO that has escaped from the electrode at −0.60, −0.65, −0.70, −0.75, −0.80 V vs RHE in a 1 h electrochemical experiment in 0.1 M $KHCO_3$, 20 mL/min (filled), 5 mL/min CO_2 flow rate (hollow), AgCu (red), and PdCu (blue). Data used are from a GC injection 15 min into the electrochemical experiment.

Figure 3 shows that at −0.6 to −0.7 V and low flow where both nanozymes are stable,[15] the AgCu nanozymes produced more CO at all potentials investigated (open red and blue circles for AgCu and PdCu nanozyme, respectively) and hence more C_3 products such as propanol. The appearance of C_3 products under these conditions suggests that the high CO levels in the nanoconfined spaces bias the reduction reaction via the CO insertion mechanism, where a CO molecule inserts into an already surface-bound species.[29] The lower CO production at low CO_2 flow explains why C_3 products are not observed on the PdCu nanozymes until −0.8 V. This is supported by the Pd core producing less CO compared with the Ag core instead producing far more H_2 (Figures S15 and S16).

At high CO_2 flow, both nanozymes had similar amounts of CO leaving the nanozymes at −0.6 to −0.65 V which was also similar to the AgCu nanozyme at low flow (filled and open red circles for AgCu at 20 and 5 mL min^{-1}, respectively, and filled blue circles for PdCu at 20 mL min^{-1}). However, at higher flow, there was an increase in the amount of CO detected at −0.7 and −0.75 V for the AgCu nanozyme (filled red circles). This is attributed to the CO production becoming faster as the destruction of the Cu shell causes more of the Ag core surface to be exposed. This accelerates the destruction of the shell and causes a large increase in CO leaving the electrode.[15]

At −0.7 and −0.75 V, the amount of CO leaving the PdCu nanozyme remained constant at the higher CO_2 flow (close blue circles). This is in part due to the Pd core becoming more selective at producing formate instead of CO over these potentials, as shown in Figure S17. However, the greater production of C_{2+} products at higher overpotentials strongly suggests that the Pd core is still producing greater amounts of CO at more negative overpotentials and that more of the produced CO is being utilized to form C_{2+} products. It is the Pd core production of formate and the greater utilization of the intermediate CO which causes the apparent stagnation in CO leaving the electrode at higher overpotentials.

With these different conditions achieved using our three main variables, the core, the CO_2 flow and the potential, we next looked in more detail at the product distribution to see if they are aligned with the expected products in Scheme 2.[29] Figure 4 shows the product distribution of ethylene, ethane, acetate, and propanol under all tested conditions.

The first major group of products is the oxygenated products that form through a CO insertion mechanism highlighted by the top (green) pathways in Scheme 2. This group of products requires high enough CO concentrations within the nanoconfined shell in order to promote this CO insertion mechanism.[29] This is the case for the AgCu nanozyme in the region where it performs a stable cascade at low flow and −0.65 V. Under these conditions, the AgCu nanozyme produced both acetate and propanol (open red circles in Figure 4a,b, respectively). Note that propanol was the only C_3 product observed. At −0.8 V, we also saw an increase in the formation of these products, but this is attributed to direct CO_2 reduction on Cu that becomes active at higher overpotentials.[40] Additionally, at these higher overpotentials, uncertainties increase due to the large gas generation from both the Ag and Pd cores producing CO and H_2. Based on this, we can conclude that the AgCu nanozyme with low flow

https://doi.org/10.1021/acs.jpcc.2c07518
J. Phys. Chem. C 2023, 127, 289−299

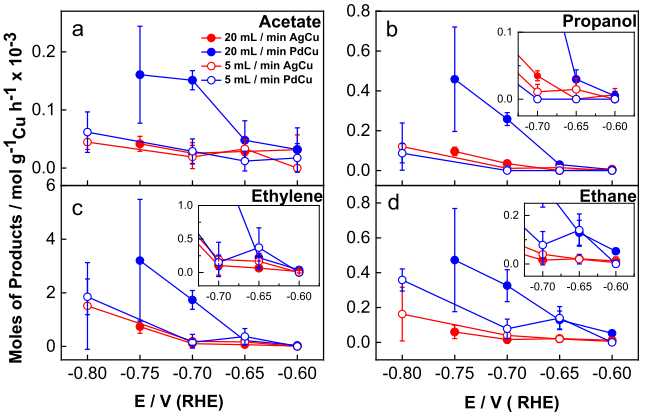

Figure 4. Moles of ethylene (a), ethane (b), acetate (c), and propanol (d) produced per gram of Cu at −0.60, −0.65, −0.70, −0.75, and −0.80 V vs RHE in a 1 h electrochemical experiment in 0.1 M $KHCO_3$ with 5 mL/min (open), 20 mL/min (filled), AgCu (red), and PdCu (blue).

and at −0.65 V produced CO at a high enough rate to keep the concentrations within the nanoconfined shell required to promote CO insertion reactions. The PdCu at low flow does not produce CO at a rate suitable to promote the formation of these oxygenated products, and only products that do not require CO insertion such as ethane and ethylene are observed.

The second major group of products are non-oxygenated hydrocarbon products, as shown with the left (blue) pathway in Scheme 2. It has previously been reported that more confined geometries which are theorized to increase OH^- local concentrations promote the formation of hydrocarbon products such as ethylene and ethane.[32] With the PdCu nanozyme at low flow, we see a preference for this pathway due to the low concentration of CO within the nanoconfined Cu shell as well as the high pH caused by the Pd core HER activity. This results in the increased production at −0.65 V for ethylene and ethane, as shown in Figure 4c,d, respectively, at the PdCu relative to the AgCu nanozyme.

With the PdCu nanozyme at high flow, we are in a different mechanistic regime from the lower CO_2 flow, as suggested by the overall increased C_2 and the formation of C_3 products as well as the differences in methane production (Figure S18). At high flow, the PdCu nanozyme produced CO in similar quantities to the AgCu nanozyme at −0.65 and low flow (Figure 3) and as such form oxygenated products in comparable quantities. The difference is that at high overpotentials, at the Pd cores, the more constant CO production as a function of potential results in the PdCu nanozyme being able to utilize the increasing overpotential to convert the smaller amount of intermediate CO into higher-order products, resulting in more C_2 and C_3 product formation at higher overpotentials. Additionally, HER on the Pd core alters the local solution environment, increasing the pH and promoting the formation of C_2 products.[3,35] The preferential formation of hydrocarbons such as ethylene and ethane implies a C−O scission occurring after the formation of oxygenation hydrocarbon intermediates. The higher hydrocarbon levels on the PdCu than the AgCu at all potentials suggest that the pH effect is not potential dependent across the measured potentials. In both cases, conditions that result in higher CO* coverage result in production of more oxygenated products due to less surface being available for H* adsorption.[3] If this is the case, the effect of the pH change from the Pd core is maximized at low flow due to the lower CO coverage, resulting in more *H adsorption and therefore more HER increasing the pH, resulting in increased selectivity for C_2 products.

In summary, we show using the cascade nanozyme system where there are spatially separated active sites allow for control over the solution conditions in nanoconfined spaces, providing control over the reaction products generated in an analogous manner to enzymes. In the cascade nanozyme system, using either AgCu or PdCu nanozymes for the CO_2RR, the control of reactant delivery to the first active site is achieved through the flow of CO_2. Control over the amount of CO intermediate in solution and the pH of the solution inside the nanoconfined spaces is achieved through altering the catalytic activity of the core via changing the metal. However, the potential provides control over the reaction of intermediate species in the Cu shell to produce higher order hydrocarbons. Together control of reactant delivery, intermediate concentration, and solution pH then provides control over the distribution of products generated by the bimetallic cascade CO_2RR and allows the production of more complex products at lower overpotentials than achievable with systems without the control over the solution environment provided by the nanoconfinement. The ability to use nanoconfinement to alter the solution environment inside the mesoporous domains then allows us to achieve the surprising result that the less active catalyst for the production of CO from CO_2, the PdCu nanozyme, has the ability to form more of the higher order hydrocarbon products, including C_3 products while maintaining the Cu structure stability. We demonstrate for the first time in an electrochemical CO_2 reduction spill-over process that by controlling the solution environment, a less active first active site provides increased C_{2+} product formation. As the less active catalyst for producing CO also possesses greater stability, we show that nanoconfinement can be used to get the best of both worlds with regard to have a stable catalyst with high activity. We hope that this study also serves as an inspiration to others to more actively explore ways of controlling the solution environment using nanoconfinement as well as more material development and theoretical modeling focusing on nanoconfined spill-over mechanisms to improve the electrochemical reactions.

■ ASSOCIATED CONTENT

Supporting Information

The Supporting Information is available free of charge at https://pubs.acs.org/doi/10.1021/acs.jpcc.2c07518.

Low-resolution TEM characterization with size distributions, detailed breakdown of CO_2RR products with uncertainties, and HRTEM analysis of particles before and after catalysis (PDF)

■ AUTHOR INFORMATION

Corresponding Authors

Richard D. Tilley − *Electron Microscope Unit, Mark Wainwright Analytical Centre and School of Chemistry and Australian Centre for NanoMedicine, University of New South Wales, Sydney 2052, Australia;* orcid.org/0000-0003-2097-063X; Email: r.tilley@unsw.edu.au

J. Justin Gooding − *School of Chemistry and Australian Centre for NanoMedicine, University of New South Wales,*

https://doi.org/10.1021/acs.jpcc.2c07518
J. Phys. Chem. C 2023, 127, 289−299

Sydney 2052, Australia; orcid.org/0000-0002-5398-0597; Email: justin.gooding@unsw.edu.au

Authors

Samuel V. Somerville − *School of Chemistry and Australian Centre for NanoMedicine, University of New South Wales, Sydney 2052, Australia;* orcid.org/0000-0003-1810-285X

Peter B. O'Mara − *School of Chemistry and Australian Centre for NanoMedicine, University of New South Wales, Sydney 2052, Australia*

Tania M. Benedetti − *School of Chemistry and Australian Centre for NanoMedicine, University of New South Wales, Sydney 2052, Australia;* Present Address: School of Environment and Science—Chemical Sciences, Griffith University, Brisbane 4111, Queensland, Australia

Soshan Cheong − *Electron Microscope Unit, Mark Wainwright Analytical Centre, University of New South Wales, Sydney 2052, Australia;* orcid.org/0000-0001-6133-0829

Wolfgang Schuhmann − *Analytical Chemistry—Center for Electrochemical Sciences (CES), Faculty of Chemistry and Biochemistry, Ruhr-Universität Bochum, Bochum D-44780, Germany;* orcid.org/0000-0003-2916-5223

Complete contact information is available at: https://pubs.acs.org/10.1021/acs.jpcc.2c07518

Author Contributions

The manuscript was written through contributions of all authors.

Notes

The authors declare no competing financial interest.

■ ACKNOWLEDGMENTS

This research was financially supported by the Australian Research Council Discovery Projects (DP210102698 to J.J.G. and DP190102659 to R.D.T.) and the Mark Wainwright Analytical Centre (MWAC) at UNSW. This work used the facilities supported by Microscopy Australia at the Electron Microscope Unit at UNSW. S.V.S. and P.B.O'M. acknowledge the Australian Government Research Training Program Scholarship for financial support. W.S. acknowledges the European Research Council (ERC) under the European Union's Horizon 2020 research and innovation program [CasCat (833408)].

■ ABBREVIATIONS

CO_2RR, carbon dioxide reduction reaction; C_x product, carbon dioxide reduction reaction product with x carbons, C_{2+} denotes C_2 and C_3 products; RHE, reversible hydrogen electrode; HER, hydrogen evolution reaction; TEM, transmission electron microscopy; EDX, energy-dispersive X-ray spectroscopy; HRTEM, high-resolution transmission electron microscopy; STEM, scanning transmission electron microscopy

■ REFERENCES

(1) Montoya, J. H.; Seitz, L. C.; Chakthranont, P.; Vojvodic, A.; Jaramillo, T. F.; Nørskov, J. K. Materials for Solar Fuels and Chemicals. *Nat. Mater.* **2016**, *16*, 70−81.

(2) Nitopi, S.; Bertheussen, E.; Scott, S. B.; Liu, X.; Engstfeld, A. K.; Horch, S.; Seger, B.; Stephens, I. E. L.; Chan, K.; Hahn, C.; et al. Progress and Perspectives of Electrochemical CO2 Reduction on Copper in Aqueous Electrolyte. *Chem. Rev.* **2019**, *119*, 7610−7672.

(3) Wang, L.; Nitopi, S. A.; Bertheussen, E.; Orazov, M.; Morales-Guio, C. G.; Liu, X.; Higgins, D. C.; Chan, K.; Nørskov, J. K.; Hahn, C.; et al. Electrochemical Carbon Monoxide Reduction on Polycrystalline Copper: Effects of Potential, Pressure, and pH on Selectivity toward Multicarbon and Oxygenated Products. *ACS Catal.* **2018**, *8*, 7445−7454.

(4) Hori, Y.; Murata, A.; Takahashi, R. Formation of Hydrocarbons in the Electrochemical Reduction of Carbon Dioxide at a Copper Electrode in Aqueous Solution. *J. Chem. Soc., Faraday Trans. 1* **1989**, *85*, 2309−2326.

(5) Gao, J.; Zhang, H.; Guo, X.; Luo, J.; Zakeeruddin, S. M.; Ren, D.; Grätzel, M. Selective C-C Coupling in Carbon Dioxide Electroreduction via Efficient Spillover of Intermediates As Supported by Operando Raman Spectroscopy. *J. Am. Chem. Soc.* **2019**, *141*, 18704−18714.

(6) Huang, J.; Mensi, M.; Oveisi, E.; Mantella, V.; Buonsanti, R. Structural Sensitivities in Bimetallic Catalysts for Electrochemical CO2 Reduction Revealed by Ag-Cu Nanodimers. *J. Am. Chem. Soc.* **2019**, *141*, 2490−2499.

(7) Morales-Guio, C. G.; Cave, E. R.; Nitopi, S. A.; Feaster, J. T.; Wang, L.; Kuhl, K. P.; Jackson, A.; Johnson, N. C.; Abram, D. N.; Hatsukade, T.; et al. Improved CO2 reduction activity towards C2+ alcohols on a tandem gold on copper electrocatalyst. *Nat. Catal.* **2018**, *1*, 764−771.

(8) Huang, J.; Mensi, M.; Oveisi, E.; Mantella, V.; Buonsanti, R. Structural Sensitivities in Bimetallic Catalysts for Electrochemical CO2 Reduction Revealed by Ag-Cu Nanodimers. *J. Am. Chem. Soc.* **2019**, *141*, 2490−2499.

(9) Ren, F.; Wenjian, H.; Cheng, W.; Pin, W.; Wenbo, L.; Congping, W.; Yingfang, Y.; Wenjun, L.; Zhigang, Z. An Extrinsic Faradaic Layer on CuSn for High-Performance Electrocatalytic CO_2 Reduction. *CCS Chem.* **2022**, *4*, 1610−1618.

(10) Lv, H.; Fang, L.; Huaiyu, Q.; Xiaowen, M.; Lizhi, S.; Na, H.; Dongdong, X.; Yanguang, L.; Ben, L. Single-Crystalline Mesoporous Palladium and Palladium-Copper Nanocubes for Highly Efficient Electrochemical CO_2 Reduction. *CCS Chem.* **2022**, *4*, 1376−1385.

(11) Benedetti, T. M.; Andronescu, C.; Cheong, S.; Wilde, P.; Wordsworth, J.; Kientz, M.; Tilley, R. D.; Schuhmann, W.; Gooding, J. J. Electrocatalytic Nanoparticles That Mimic the Three-Dimensional Geometric Architecture of Enzymes: Nanozymes. *J. Am. Chem. Soc.* **2018**, *140*, 13449−13455.

(12) Gooding, J. J. Can Nanozymes Have an Impact on Sensing? *ACS Sens.* **2019**, *4*, 2213−2214.

(13) Scott, S.; Zhao, H.; Dey, A.; Gunnoe, T. B. Nano-Apples and Orange-Zymes. *ACS Catal.* **2020**, *10*, 14315−14317.

(14) O'Mara, P. B.; Wilde, P.; Benedetti, T. M.; Andronescu, C.; Cheong, S.; Gooding, J. J.; Tilley, R. D.; Schuhmann, W. Cascade Reactions in Nanozymes: Spatially Separated Active Sites inside Ag-Core-Porous-Cu-Shell Nanoparticles for Multistep Carbon Dioxide Reduction to Higher Organic Molecules. *J. Am. Chem. Soc.* **2019**, *141*, 14093−14097.

(15) Wilde, P.; O'Mara, P. B.; Junqueira, J. R. C.; Tarnev, T.; Benedetti, T. M.; Andronescu, C.; Chen, Y. T.; Tilley, R. D.; Schuhmann, W.; Gooding, J. J. Is Cu instability during the CO2 reduction reaction governed by the applied potential or the local CO concentration? *Chem. Sci.* **2021**, *12*, 4028−4033.

(16) Ma, M.; Trześniewski, B. J.; Xie, J.; Smith, W. A. Selective and Efficient Reduction of Carbon Dioxide to Carbon Monoxide on Oxide-Derived Nanostructured Silver Electrocatalysts. *Angew. Chem., Int. Ed.* **2016**, *55*, 9748−9752.

(17) Hori, Y.; Wakebe, H. H. I.; Tsukamoto, T.; Koga, O. Electrocatalytic process of CO selectivity in electrochemical reduction of CO2 at metal electrodes in aqueous media. *Electrochim. Acta* **1994**, *39*, 1833−1839.

(18) Hansen, H. A.; Varley, J. B.; Peterson, A. A.; Nørskov, J. K. Understanding Trends in the Electrocatalytic Activity of Metals and Enzymes for CO2 Reduction to CO. *J. Phys. Chem. Lett.* **2013**, *4*, 388−392.

(19) Angulo, A.; van der Linde, P.; Gardeniers, H.; Modestino, M.; Fernández Rivas, D. Influence of Bubbles on the Energy Conversion Efficiency of Electrochemical Reactors. *Joule* **2020**, *4*, 555−579.
(20) Chen, B.; Jiao, X.; Chen, D. Size-Controlled and Size-Designed Synthesis of Nano/Submicrometer Ag Particles. *Cryst. Growth Des.* **2010**, *10*, 3378−3386.
(21) Chen, H.; Wei, G.; Ispas, A.; Hickey, S. G.; Eychmüller, A. Synthesis of Palladium Nanoparticles and Their Applications for Surface-Enhanced Raman Scattering and Electrocatalysis. *J. Phys. Chem. C* **2010**, *114*, 21976−21981.
(22) Zhang, L.; Jing, H.; Boisvert, G.; He, J. Z.; Wang, H. Geometry Control and Optical Tunability of Metal-Cuprous Oxide Core-Shell Nanoparticles. *ACS Nano* **2012**, *6*, 3514−3527.
(23) Alinezhad, A.; Gloag, L.; Benedetti, T. M.; Cheong, S.; Webster, R. F.; Roelsgaard, M.; Iversen, B. B.; Schuhmann, W.; Gooding, J. J.; Tilley, R. D. Direct Growth of Highly Strained Pt Islands on Branched Ni Nanoparticles for Improved Hydrogen Evolution Reaction Activity. *J. Am. Chem. Soc.* **2019**, *141*, 16202−16207.
(24) Masa, J.; Schuhmann, W. Electrocatalysis and bioelectrocatalysis - Distinction without a difference. *Nano Energy* **2016**, *29*, 466−475.
(25) Kelly, C. H. W.; Benedetti, T. M.; Alinezhad, A.; Gooding, J. J.; Tilley, R. D. Controlling Metallic Nanoparticle Redox Properties for Improved Methanol Oxidation Reaction Electrocatalysis. *ChemCatChem* **2019**, *11*, 5989−5993.
(26) Jouny, M.; Luc, W.; Jiao, F. High-Rate Electroreduction of Carbon Monoxide to Multi-Carbon Products. *Nat. Catal.* **2018**, *1*, 748−755.
(27) Schouten, K. J. P.; Pérez Gallent, E.; Koper, M. T. M. The influence of pH on the reduction of CO and CO2 to hydrocarbons on copper electrodes. *J. Electroanal. Chem.* **2014**, *716*, 53−57.
(28) Romero Cuellar, N. S.; Wiesner-Fleischer, K.; Fleischer, M.; Rucki, A.; Hinrichsen, O. Advantages of CO over CO2 as reactant for electrochemical reduction to ethylene, ethanol and n-propanol on gas diffusion electrodes at high current densities. *Electrochim. Acta* **2019**, *307*, 164−175.
(29) Zheng, Y.; Vasileff, A.; Zhou, X.; Jiao, Y.; Jaroniec, M.; Qiao, S.-Z. Understanding the Roadmap for Electrochemical Reduction of CO2 to Multi-Carbon Oxygenates and Hydrocarbons on Copper-Based Catalysts. *J. Am. Chem. Soc.* **2019**, *141*, 7646−7659.
(30) Wordsworth, J.; Benedetti, T. M.; Alinezhad, A.; Tilley, R. D.; Edwards, M. A.; Schuhmann, W.; Gooding, J. J. The Importance of Nanoscale Confinement to Electrocatalytic Performance. *Chem. Sci.* **2020**, *11*, 1233−1240.
(31) Sen, S.; Liu, D.; Palmore, G. T. R. Electrochemical Reduction of CO2 at Copper Nanofoams. *ACS Catal.* **2014**, *4*, 3091−3095.
(32) Yang, K. D.; Ko, W. R.; Lee, J. H.; Kim, S. J.; Lee, H.; Lee, M. H.; Nam, K. T. Morphology-Directed Selective Production of Ethylene or Ethane from CO 2 on a Cu Mesopore Electrode. *Angew. Chem., Int. Ed.* **2017**, *56*, 796−800.
(33) Ting, L. R. L.; Yeo, B. S. Recent Advances in Understanding Mechanisms for the Electrochemical Reduction of Carbon Dioxide. *Curr. Opin. Electrochem.* **2018**, *8*, 126−134.
(34) Gauthier, J. A.; Lin, Z.; Head-Gordon, M.; Bell, A. T. Pathways for the Formation of C2+ Products under Alkaline Conditions during the Electrochemical Reduction of CO2. *ACS Energy Lett.* **2022**, *7*, 1679−1686.
(35) Liu, X.; Schlexer, P.; Xiao, J.; Ji, Y.; Wang, L.; Sandberg, R. B.; Tang, M.; Brown, K. S.; Peng, H.; Ringe, S.; et al. pH Effects on the Electrochemical Reduction of CO_2 towards C_2 Products on Stepped Copper. *Nat. Commun.* **2019**, *10*, 32.
(36) Kortlever, R.; Shen, J.; Schouten, K. J. P.; Calle-Vallejo, F.; Koper, M. T. M. Catalysts and Reaction Pathways for the Electrochemical Reduction of Carbon Dioxide. *J. Phys. Chem. Lett.* **2015**, *6*, 4073−4082.
(37) Pang, Y.; Li, J.; Wang, Z.; Tan, C. S.; Hsieh, P. L.; Zhuang, T. T.; Liang, Z. Q.; Zou, C.; Wang, X.; De Luna, P.; et al. Efficient Electrocatalytic Conversion of Carbon Monoxide to Propanol Using Fragmented Copper. *Nat. Catal.* **2019**, *2*, 251−258.
(38) Li, C. W.; Kanan, M. W. CO2Reduction at Low Overpotential on Cu Electrodes Resulting from the Reduction of Thick Cu2O Films. *J. Am. Chem. Soc.* **2012**, *134*, 7231−7234.
(39) Zhuang, T. T.; Pang, Y.; Liang, Z. Q.; Wang, Z.; Li, Y.; Tan, C. S.; Li, J.; Dinh, C. T.; De Luna, P.; Hsieh, P. L.; et al. Copper nanocavities confine intermediates for efficient electrosynthesis of C3 alcohol fuels from carbon monoxide. *Nat. Catal.* **2018**, *1*, 946−951.
(40) Han, J.; Long, C.; Zhang, J.; Hou, K.; Yuan, Y.; Wang, D.; Zhang, X.; Qiu, X.; Zhu, Y.; Zhang, Y.; et al. A reconstructed porous copper surface promotes selectivity and efficiency toward C2 products by electrocatalytic CO2 reduction. *Chem. Sci.* **2020**, *11*, 10698−10704.

https://doi.org/10.1021/acs.jpcc.2c07518
J. Phys. Chem. C 2023, 127, 289−299